Characterization of the Microstructure after Composite Peening of Aluminum

Michael Seitz,* Michael Dürrschnabel, Alexander Kauffmann, Chantal Kurpiers, Christian Greiner, and Kay André Weidenmann

Composite peening is a novel process to introduce ceramic blasting particles into the surface of substrates. Depending on the process parameters, the penetration depth of the blasting particles can be several micrometers. In previous investigations by some of the authors, it has been found that the ceramic particles incorporated during composite peening are significantly smaller compared to 10 μm in size before peening. Herein, the microstructure after composite peening is highlighted. To investigate this microstructure, scanning electron microscopy (SEM) and transmission electron microscopy (TEM) are performed. The subsequent X-ray diffraction (XRD) analysis provides further evidence of a severely deformed, nanocrystalline ceramic layer consisting of fragmented blasting particles.

1. Introduction

The purpose of composite peening is to introduce ceramic dispersoids by a micropeening process into near-surface regions of aluminum alloys to generate a graded metal matrix composite. It was observed that particle embedding by micropeening is possible and doing so an increase in hardness was achieved.[1] The authors have demonstrated that heating the peened sample during the micropeening process increases the penetration depth of the ceramic blasting particles.[2,3] The embedded particles may act as a reinforcement of the surface regions similar to coating processes such as cold gas spraying. This may lead to an enhancement in mechanical or tribological properties.

Previous investigations on commercially available, pure Al (Al 1050 alloy) showed that a hill–valley profile is formed on the surface as a result of composite peening. Embedded ceramic particles are mainly found in the valleys. At temperatures close to the solidus temperature T_s (homologous temperature $T/T_s = 0.95$), it is possible to introduce alumina particles to a depth of up to 30 μm. The ceramic particles could be found in isolated regions and were significantly smaller compared to the original size.[2]

Research in the field of solid particle erosion is closely related to research on shot peening and composite peening. Although these investigations are primarily focused on describing erosion phenomena and avoiding erosion, the devices used to investigate erosion behavior are similar to those used for shot peening. For example, air-blast erosion testers, free-fall testers, and wheel blast methods are used,[4] which are also used in applications of shot peening.[5] In addition to the similarities in the experimental setups, many investigations in the field of solid particle erosion discussed in the following also show that fragments of the erosion particles remain stuck and/or are embedded.[6–14] Different substrates such as Al, Cu, and polymers were subjected to ceramic erosion particles.

Brown et al.[6] observed a distinct hill–valley profile of the eroded surface of the Al 1100 base material after the erosion process. A minimum particle size of 20 μm was assumed to be required to form such a profile. While smaller (70 μm) silica spheres showed no embedding, larger (210 μm) erodent fragments of the abrasive silica and quartz were found embedded in near-surface regions. In the case of the angular quartz particles, pockets of ceramic fragments were found which were separated by regions without embedded particles. The investigations published in Doyle and Levy[7] are focused on the erosion behavior of Al 1100 at elevated temperatures up to a homologous temperature of 0.8. At an incident angle of 90°, the SiC particles (250–300 μm) form patterns of hills and valleys and embedded particles are found in the valleys. While a comparably high velocity of the blast particles can be achieved with the jet and impeller methods, the particle velocity in the free-fall experiments of Zu et al.[8] was below 10 m s^{-1}. Nevertheless, fragments of sand particles were found in

M. Seitz, Dr. A. Kauffmann
Institute for Applied Materials (IAM-WK)
Karlsruhe Institute of Technology (KIT)
Engelbert-Arnold-Straße 4, 76131 Karlsruhe, Germany
E-mail: michael.seitz@kit.edu

Dr. M. Dürrschnabel
Institute for Applied Materials (IAM-AWP)
Karlsruhe Institute of Technology (KIT)
Hermann-von-Helmholtz-Platz 1, 76344 Eggenstein-Leopoldshafen, Germany

C. Kurpiers, Dr. C. Greiner
Institute for Applied Materials (IAM-CMS)
Karlsruhe Institute of Technology (KIT)
Straße am Forum 7, 76131 Karlsruhe, Germany

Prof. K. A. Weidenmann
Institute of Materials Resource Management
Augsburg University
Universitätsstraße 1, 86159 Augsburg, Germany

The ORCID identification number(s) for the author(s) of this article can be found under https://doi.org/10.1002/adem.202000575.

technically pure Al. The size of the fragmented particles found was 20 μm and significantly smaller than the initial size (600–850 μm). In addition, the particles showed numerous cracks.

Cousens and Hutchings[9] described the observation phenomena occurring during the erosion of Al under 90° by spherical particles. A hill–valley profile has been observed, which repeats at constant intervals in the order of the particle diameter. Blasting with glass beads (212–250 and 495–600 μm) formed a laminar structure of Al and fragments of the erosion particles along the surface of the sample, which can be clearly distinguished from the substrate material. By using roll-bonded specimens, it was possible to describe the deformation behavior after the composite layer was formed and the so-called steady state erosion was reached. Subsequent particles are supposed to press the harder layer into the bulk material. The resulting compressive stress in the bulk material leads to a backward extrusion process. This backward extrusion finally forms the hills of the surface topography and regions with fragments of the erosion particles.

Salik et al.[10] could not observe particle embedding for different heat treatment conditions of Al 6061. This was attributed to the low, but not further specified, velocity of the 15 μm glass spheres. The previous investigation of the erosion properties of Al and Cu showed that 15 μm large glass beads remain stuck in the surface at faster particle speeds of $93 \, \mathrm{m \, s^{-1}}$.[11] Furthermore, in the case of SiC (50 μm) used as an abrasive, visible light was emitted during the peening process, which indicates particle fracture.

TEM investigations by Edington and Wright[12] on eroded Stellite 6B showed fragments of penetrated abrasive particles in the order of 30–500 nm in a layer on the surface with an estimated thickness of 1–2 μm. The initial size of the alumina particles was 15 μm at a velocity of $52 \, \mathrm{m \, s^{-1}}$. This layer is formed from the embedded particles by subsequent peening of the following particles. The fragmented particles seem to be kept together by a kind of cobalt binder, which was identified by diffraction patterns. Tilly and Sage[13] noted by erosion with quartz particles (125–150 μm) that particles smaller than 10–20 μm do not fragment any more. Larger sized particles result in increased fragmentation.

To recapitulate, first investigations in composite peening showed a number of similarities to solid particle erosion, such as embedding of (fragmented) blasting particles. However, it was observed several times that smaller particles do not fragment or remain stuck. The reasons for this were ambiguous. Because, in contrast to solid particle erosion, the purpose of composite peening is to reinforce the surface layer, a detailed investigation of the microstructure is essential to holistically evaluate the mechanical properties. Scanning electron microscopy (SEM) and transmission electron microscopy (TEM) investigations as well as X-ray diffraction (XRD) are expected to provide detailed information to answer the question of particle fragmentation and the formation of topography due to composite peening. Furthermore, the size of the blasting particles after composite peening, the composition of the particle regions, and the bonding between the fragmented particles are central topics of this research.

2. Experimental Section

2.1. Materials

The Al 6082 alloy was used as base material. The sheet material was purchased from BIKAR-METALLE (Bad Berleburg–Raumland, Germany). The chemical composition is shown in **Table 1** and is in accordance with the DIN EN 573 standard.[15] Alumina of F600 microgrit (Arteka, Backnang–Waldrems, Germany), which corresponds to a weight-averaged grain size of $9.3 \pm 1.0 \, \mu m$, was used as blasting particles and reinforcing material. Several measurements by laser diffraction yielded a median particle size distribution of 8–13 μm. The shape of the ceramic particles was angular, as shown in **Figure 1**.

2.2. Composite Peening

Composite peening describes a process based on micropeening developed by the authors and first published in 2017.[16] A detailed description and scheme of the setup of the composite peening system is described elsewhere.[2] By adding a heating device, it was possible to introduce the blasting particles in the heated substrate material (Al 1050). The manufacturing of the samples for microstructural investigations was performed at a homologous temperature of $T/T_s = 0.9$, namely, 490 °C. The operating pressure of the micropeening system was 7 bar. The blasting nozzle with a diameter of 0.7 mm had a feed rate of $8 \, \mathrm{mm \, s^{-1}}$ at a working distance of 10 mm. A fourfold coverage with a path distance of 1 mm was used.

Composite peening significantly increases the roughness of the surface.[17] In this study, the roughness after composite

Table 1. Chemical composition of the Al 6082 alloy.

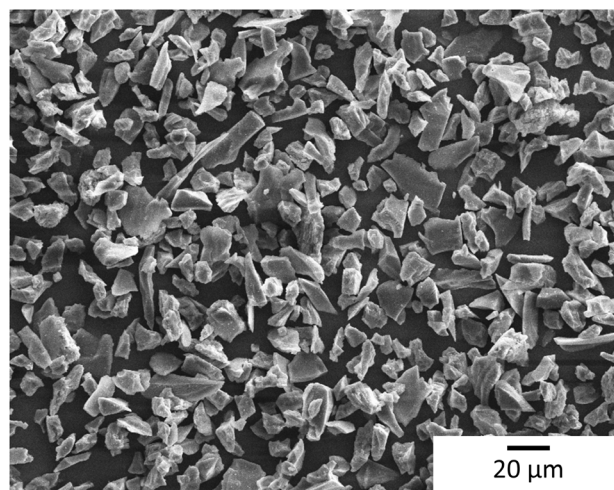| Al 6082	Al	Mg	Si	Fe	Cu	Mn	Ti	Zn
Wt%	97.15/base	0.90	0.88	0.40	0.08	0.43	0.03	0.09

Figure 1. SEM (secondary electron contrast, SE) image of the used alumina blasting particles with an angular shape.

**ADVANCED
SCIENCE NEWS**

www.advancedsciencenews.com

**ADVANCED
ENGINEERING
MATERIALS**

www.aem-journal.com

peening was $R_z = 13.7 \pm 2.0\,\mu m$, whereas $2.6 \pm 0.4\,\mu m$ was observed prior to the peening process. To close open structures near the surface created by the peening process, the samples were deep rolled at a pressure of 40 bar subsequently. Thereby the roughness was reduced to $R_z = 3.6 \pm 1.4\,\mu m$. Smoothing the surface also supports detailed examination of the surface layer by SEM and TEM. The influence of deep rolling on the ceramic particles and Al base material is discussed later.

2.3. Microstructural Characterization

The investigation of the microstructure was performed using an SEM Helios Nanolab 650 by FEI. The acceleration voltage was 2–30 kV. In addition to secondary electron (SE) and backscattered electron (BSE) contrast imaging, energy-dispersive X-ray spectroscopy (EDX) was performed. The images shown later provide a representative selection of the microstructure of the composite peened Al.

The preparation of a lamella for TEM was conducted via a focused ion beam (FIB) on the same instrument. The cross-section of the prepared lamella was 18 μm by 27 μm, thinned to around 100 nm thickness in two regions. The lamella was analyzed with a Thermo Fisher Talos F200X G2 scanning TEM (STEM) equipped with four EDX detectors and a Gatan Enfinium Electron Loss Spectrometer (EELS) with dual EELS capability. The acceleration voltage was 200 kV. The convergence and collection angle for the EELS measurements were 10.5 and 14.1 mrad, respectively. The TEM images were taken with a Thermo Fisher Ceta 16M CCD camera.

The characterization of the grain size and dislocation density of the oxide particles before and after the composite peening process was investigated by XRD on a D2 Phaser from Bruker equipped with a LynxEye line detector. The Cu X-ray tube of the diffractometer was operated at 30 kV with 10 mA. The corundum (Al_2O_3) peaks were evaluated both for the initial blasting particles and subsequent to the peening process on the substrate. The examination was performed in a range of $2\theta = 10°–145°$ with a step size of 0.01° and an accumulated acquisition time of 384 s per step. The subsequent evaluation of the diffraction patterns was performed using a superimposed Lorentz function for $K_{\alpha 1}$ and $K_{\alpha 2}$ deconvolution.

Figure 2 shows an example of a diffraction pattern of a composite peened sample. In addition to peaks of the Al base material (square symbol) α-Al_2O_3 reflections (triangle symbol) and β-Al_2O_3 reflections (circle symbol) are detected. Exclusively reflections that clearly separate from the background or the other phase are used for further evaluation. The crystallographic planes used for further evaluations are indexed for Al and Al_2O_3 in the diagram.

While the peak positions are indicative for the crystal structure, line widths provide information about the defect structure. In addition to instrumental broadening, the defect density, namely, the dislocation density, and the crystallite size have the greatest influence on the peak broadening.[18] For the following investigations, the influence of the instrumental peak broadening is not considered. Williamson and Hall[19] revealed that line broadening is dependent on a contribution by small grain size $\Delta(2\theta)_G$ and by dislocation-induced lattice distortion $\Delta(2\theta)_S$

$$\Delta(2\theta)_S = 2\epsilon \times \tan\theta \tag{1}$$

with the internal strain ϵ and

$$\Delta(2\theta)_G = \frac{k_S \times \lambda}{d_{koh} \times \cos\theta} \tag{2}$$

utilizing the Scherrer equation for sufficiently small crystallite sizes (<150 nm).[18] The unitless Scherrer constant k_S is ≈ 0.9[18] when considering the full width at half maximum (FWHM). λ specifies the wavelength of monochromatic X-rays. d_{koh} is the size of coherently scattering regions. Because of the linear superposition of the two contributions, the total line width results in

$$\Delta(2\theta) = \Delta(2\theta)_S + \Delta(2\theta)_G = 2\epsilon \times \tan\theta + \frac{k_S \times \lambda}{d_{koh} \times \cos\theta} \tag{3}$$

By introducing the scattering vector $s = 2\sin(\theta/\lambda)$ and its derivative with respect to θ $ds/d\theta \approx \Delta s/\Delta\theta = (2\cos\theta)/\lambda$ to describe the line width, the equation can be simplified to
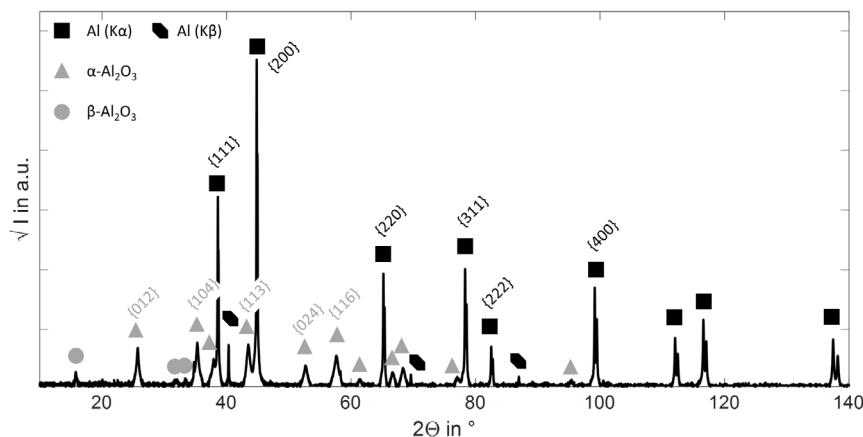

Figure 2. Diffraction pattern of a composite peened sample.

**ADVANCED
SCIENCE NEWS**

www.advancedsciencenews.com

**ADVANCED
ENGINEERING
MATERIALS**

www.aem-journal.com

$$\Delta s = \epsilon \times s + \frac{k_S}{d_{koh}} \quad (4)$$

Here, Δs corresponds to the FWHM of the peaks in terms of the scattering vector.

3. Results

3.1. SEM

The composite peening creates a hill–valley profile on the surface, as shown in **Figure 3**a. The equivalent diameters of the hills vary from 30 to 60 μm. The process of hill formation by eroding is described in the literature. Subsequent deep rolling, as shown in Figure 3b, can level the surface. Nevertheless, the valleys are still recognized as rifts and boundaries between the former hills.

A detailed micrograph of the surface after composite peening and after additional deep rolling is given in **Figure 4**. The distinct hill–valley profile after composite peening is evident. These hills are levelled by the subsequent deep rolling process. Numerous small fragments of the ceramic blasting particles are observed on both surfaces. These fragments are primarily found in the valleys of both surfaces. The largest particles on both surfaces are smaller than the initial size of the blasting particles.

Figure 5 shows a representative cross-section of the composite peened surface after FIB milling. Figure 5a shows the position of the cross-section located on a former hill indicated by the deposited Pt bar. In Figure 5b some darker regions are observed surrounded by thin, bright borders. Further investigations with EDX indicate that these darker regions consist of Al and O. The thickness of these regions varies over the entire section. On the left side of the image, Al_2O_3 with no connection to the surface is observed, indicative of a deep penetration process (white rectangle). The penetration depth in this image is almost 10 μm. In addition, there are some smaller regions of Al_2O_3 close to the surface with a very small penetration depth (white arrows). The detailed view of an Al_2O_3 area in Figure 5c reveals pores and cracks within the particle field, which otherwise appears homogeneous at lower magnifications. The fine cracks and pores can be seen in any particle-consisting region.
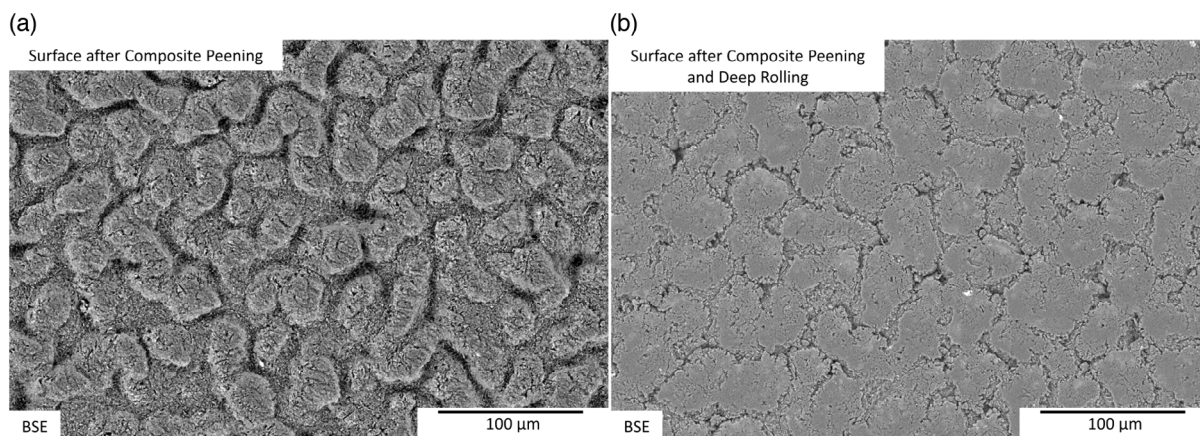

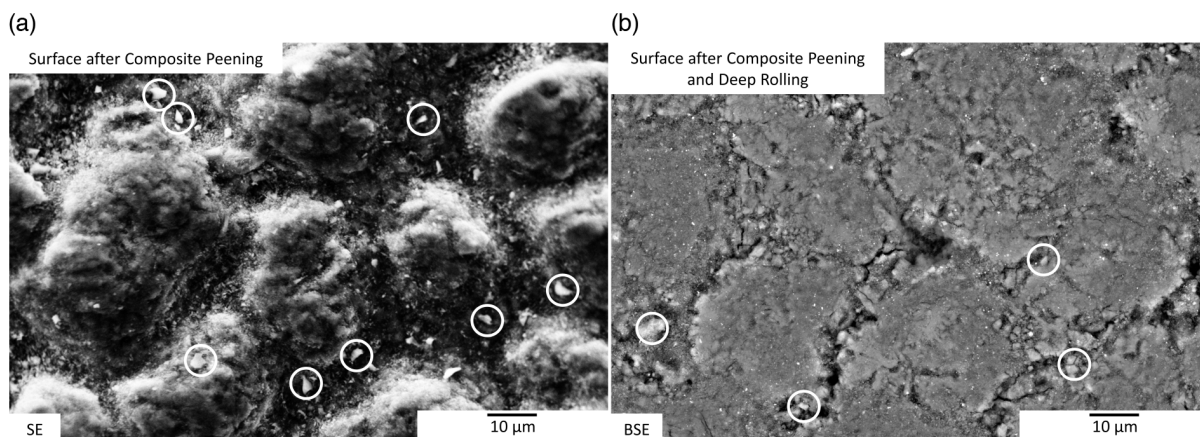**Figure 3.** SEM-BSE images of a) as-peened surface and b) after subsequent deep rolling.

Figure 4. a) Detailed SEM images of as-peened surface and b) after subsequent deep rolling. Fragmented Al_2O_3 particles are evident on both surfaces (white circles). Before deep rolling, a distinct hill–valley profile is recognizable on the surface. Deep rolling significantly levels these hills.
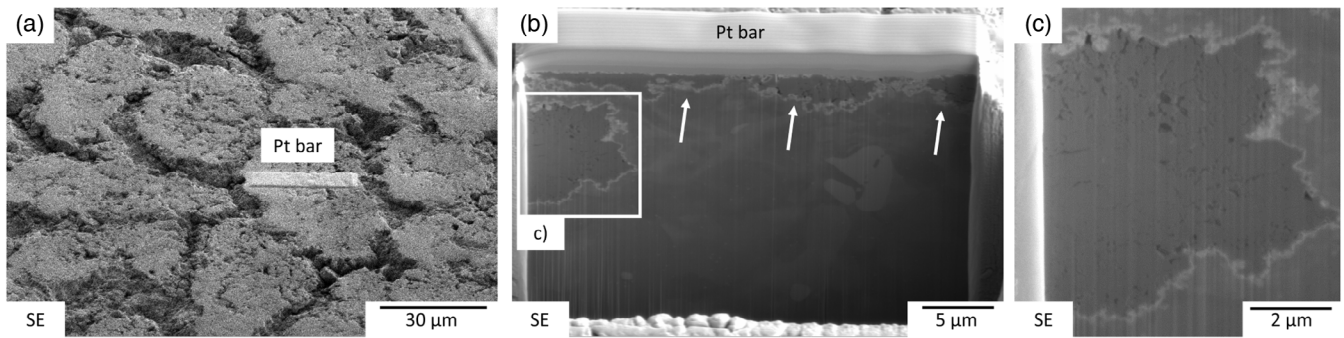
ADVANCED
SCIENCE NEWS
www.advancedsciencenews.com

ADVANCED
ENGINEERING
MATERIALS
www.aem-journal.com

Figure 5. a) Position of the FIB cross-section indicated by the Pt bar. b) FIB cross-section. The Al_2O_3 regions can be recognized by the white seam and the darker contrast. c) Detailed view of a particle segment out of (b).

3.2. TEM

A more detailed examination of the individual particle fields is conducted by means of TEM. **Figure 6** shows a particle region located directly at the surface of the composite peened specimen. The elemental maps in Figure 6 provide an overview of the distribution of Al, O, and Mg. The region in the lower part of the image is the Al base material; the upper section consists of Al and O. Quantitative EDX and quantitative EELS both give a stoichiometry of the oxide of $\approx$40:60 for Al and O and points to Al_2O_3, consequently. At the interface between Al_2O_3 and the Al base material, a significant increase in the Mg concentration is observed, as shown in the overlay in Figure 6. This is often described in the literature and indicates the formation of spinel at the interface.[20]

In scanning transmission dark-field (STEM-DF) mode, it is observed that the Al_2O_3 region is inhomogeneous. Fine marbled regions (1) are present and (2) particles in the range of almost 1 μm. Furthermore, (3) pores are found between some particles and (4) a crack separates two regions from each other. Sample thickness measurements by STEM–EELS confirm the existence of pores and cracks. Within larger particles, a change in contrast is detected indicative of severe deformations of the particles. A micrograph of section (5) at high magnification in **Figure 7** reveals a large dislocation density within single Al grains. After deep rolling, this high dislocation density in the Al base material is also detected in XRD analyses, shown in Section 3.3.

Figure 8a shows a bright-field TEM image of the Al/Al_2O_3 interface region. The TEM dark-field inset image highlights the small crystallite size in the Al_2O_3, which was found to be $\approx$25 nm for the largest grains present in this particular region. In Figure 8b the selected area electron diffraction (SAED) pattern confirms by its ring structure that the there are numerous particles in this section.
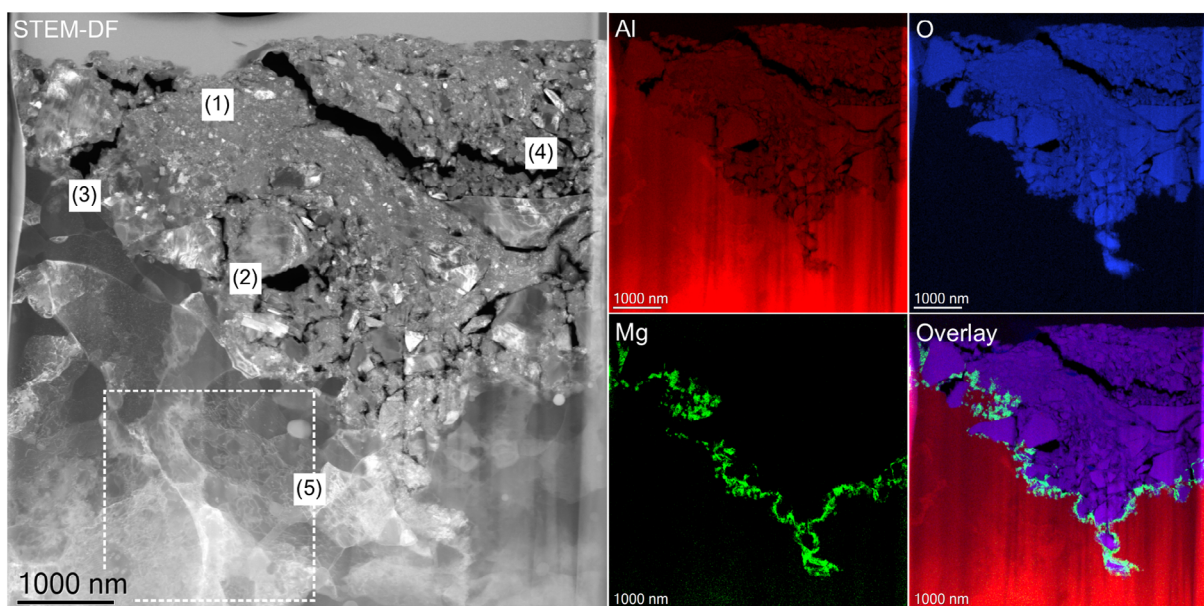

Figure 6. STEM-DF electron image of a composite peened sample. In the upper part, fine marbled areas consisting of a large number of Al_2O_3 particles can be seen. EDX elemental maps for Al, O, and Mg as well as an overlay of all three maps are shown on the right. The marked area in section (5) is shown in detail in Figure 7.
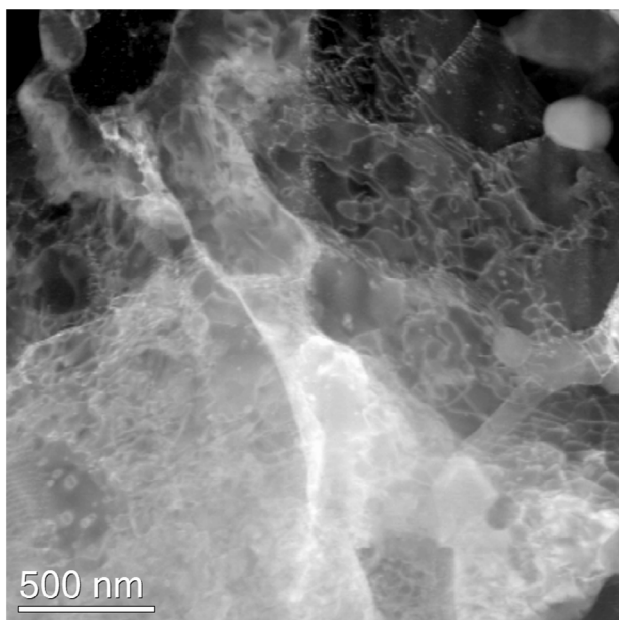
Figure 7. Enlargement of section (5) shown in Figure 6: a distinct dislocation structure is observed in the Al base material after composite peening and deep rolling.

3.3. XRD

Figure 9 shows the Williamson–Hall (WH) plot of the as-received alumina particles (left side), after composite peening and after composite peening with subsequent deep rolling. According to Equation (4), the reciprocal value of the Δs intercept can be used to calculate the average crystallite size, while the slope gives an estimate of the dislocation density. It can be seen that the slope of the particles after composite peening is larger than the slope of the particles in the initial state. The two gradient triangles illustrate the slopes for dislocation densities of 10^{13} and $10^{16}\,\mathrm{m}^{-2}$,

respectively. The dislocation density of Al_2O_3 was determined by using the approach of Williamson and Smallman[21] and assuming prism plane dislocations only, dissociated into three collinear partials with a Burgers vector of 0.274 nm.[22] The subsequent deep rolling process does not significantly change the width of the X-ray reflections. An evaluation at the {012} and {024} planes of the alumina yields a crystallite size of 110 nm in the initial state, whereas after composite peening and deep rolling a crystallite size smaller than 100 nm is determined.

In contrast to the Al_2O_3 particles, a significantly increased dislocation density can be detected in the Al base material due to deep rolling, as shown on the right side in Figure 9. A Burgers vector of 0.286 nm is used for evaluation. The evaluation of the crystallite size is not suitable for Al in this case.

4. Discussion

Similar to solid particle erosion, ceramic particles are introduced into the softer base material during composite peening. In previous investigations, it was observed that the temperature of the process and, thus, the mechanical properties of the base material play a major role in the penetration depth of the process.[2] This is consistent with earlier studies on solid particle erosion. The penetration of blasting particles in previous investigations occured unter certain conditions either to a higher impact energy due to larger particle sizes,[6,9,13] higher velocities,[10–12] or due to a lower mechanical resistance of the base material.[7]

For composite peening, a hill–valley profile can also be identified, as in some solid particle erosion investigations. The minimum particle size of $\approx 20\,\mu m$ proposed by Brown et al.[6] for the appearance of this topography was falsified in the current investigations. The evidence that smaller particles also form hill–valley profiles leads to the conclusion that, in addition to particle size, impact energy and resistance of the bulk material play a crucial role in the embedding process of the blasting particles and formation of the topography of the peened surface.
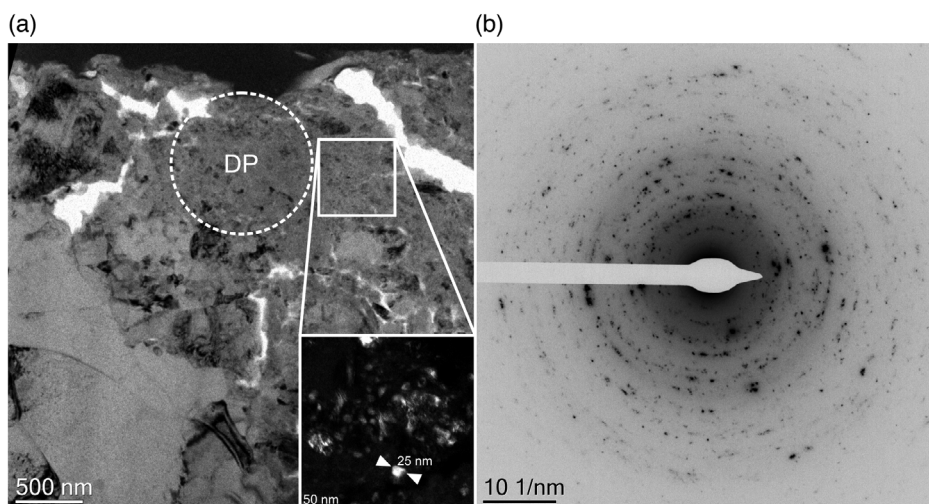

Figure 8. a) Bright-field TEM image of the Al/Al_2O_3 interface region. The inset shows a TEM dark-field image highlighting the crystallite size in the Al_2O_3 region. b) SAED pattern of the circular region marked with "DP" in (a) indicating numerous particles in the Al_2O_3 region.
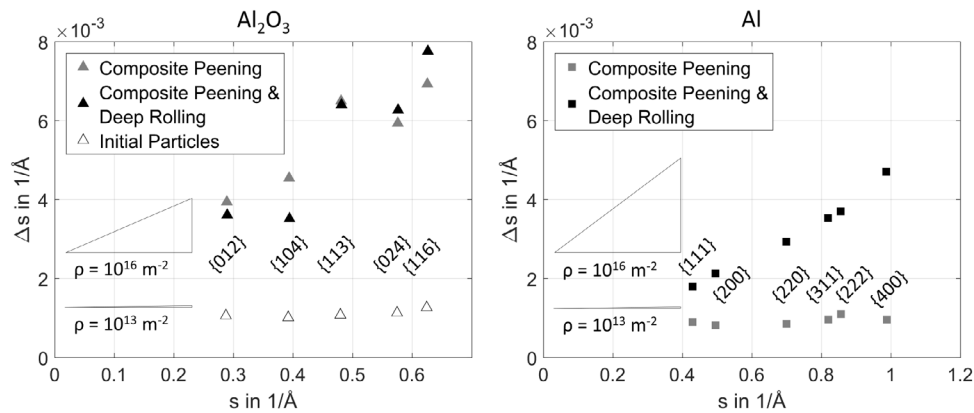
Figure 9. WH plot for Al_2O_3 and Al before and after deep rolling.

The fact that the embedded blasting particles are present as fragments is well known and documented in earlier studies.[6–9,11–13] The size of the individual fragments could not be determined unambiguously for composite peening so far. TEM investigations show Al_2O_3 particles in the surface layer down to a size within the nanometer range. This measurement is not an isolated case as proven by the evaluation of the XRD by the WH method. Here a reduction in the size of coherently scattering domains is detected after the peening process. Edington and Wright[12] also found embedded fragments in the size from 30 to 500 nm in Stellite 6B. However, the embedded fragments only reached a depth of 1–2 µm. With the process parameters used here, ceramic particles can be observed at a depth of 10 µm after composite peening (Figure 5b) and thus significantly deeper.

Both, the STEM-DF image (Figure 6) and the slope in the WH diagram (Figure 9) indicate that there is a very high defect density within the ceramic particles. However, subsequent deep rolling has no significant effect on the defect density and size of the alumina particles. The Al base material, in contrast, bears plastic deformation, as can be seen from the larger slopes caused by deep rolling in the WH plot and the high dislocation density in the TEM image (Figure 7).

Although Al_2O_3 can generally be considered as brittle at temperatures below 1000 °C, heavy plastic deformation of Al_2O_3 was detected at room temperature under certain conditions. Hockey[23] and Cutter and McPherson[24] were able to determine a significant increase of the dislocation density during abrasion by means of TEM and XRD, respectively. A grain size of 30 nm and a dislocation density of 10^{15} m^{-2} in the damage layer, similar to the dislocation density after composite peening presented here, were found in Cutter and McPherson.[24] High defect densities of Al_2O_3 have also been observed in high-dynamic processes such as ball milling[25] and explosive shock loading[26] of Al_2O_3 powder, the reasons for which are locally high hydrostatic pressures. A similar circumstance might also be considered for the composite peening process.

Noteworthy is the observation that by using EDX no Al can be found as binder phase between the individual nanoscale Al_2O_3 particles. The EDX results are confirmed by additional quantitative EELS (Figure S3, Supporting Information).

This is in contrast to the assumption of Edington and Wright[12] as well as Cousens and Hutchings,[9] who suppose binding layers of Co or Al between the individual particles accounting for the integrity of the structure. Rather, cold welding of the oxide particles is seen, which might be caused by the large plastic deformation of the oxides and assisted by the elevated temperatures resulting from the process temperature and the energy transfer by the impact events.

5. Conclusion

For the development of the microstructure by composite peening the following conclusions can be drawn. 1) High-resolution TEM images provide detailed examination of the microstructure of the particle regions formed during composite peening. These particle regions consist exclusively of Al_2O_3. No Al binder is found. 2) All particles fragment during composite peening. In addition to individual larger particle fragments (<1 µm), areas with nanoscale particles can be found. 3) XRD leads to the conclusion that there is a high defect density in the ceramic particles. This defect density may be responsible for the integrity of the particle regions. 4) A hill–valley profile is formed during composite peening with fragments of the blasting particles mainly found in the valleys. 5) At the interface between the embedded blasting particles of Al_2O_3 and the base material of Al 6082 alloy, an increase of the Mg concentration is detected. This suggests the formation of spinel.

Supporting Information

Supporting Information is available from the Wiley Online Library or from the author.

Acknowledgements

2000575 (7 of 8)

Conflict of Interest

The authors declare no conflict of interest.

Keywords

[1] M. Ando, H. Kitano, H. Usami, T. Endo, in *the 10th Int. Conf. on Shot Peening Procedure*, The Shot Peener Magazine **2008**, p. 223.

[2] M. Seitz, K. A. Weidenmann, *KEM* **2019**, *809*, 73.

[3] M. Seitz, in *Symp. Mechanical Surface Treatment 2019: 8th Workshop Machine Hammer Peening* (Eds: V. Schulze), Karlsruhe, Germany **2019**, p. 85.

[4] I. Kleis, P. Kulu, *Solid Particle Erosion. Occurrence, Prediction and Control*, Springer-Verlag London Limited, London **2008**, Ch. 1.

[5] V. Schulze, *Modern Mechanical Surface Treatment. States, Stability, Effects*, Wiley-VCH, Weinheim, Germany **2006**, Ch. 2.

[6] R. Brown, S. Kosco, E. J. Jun, *Wear* **1983**, *88*, 181.

[7] P. A. Doyle, A. V. Levy, in *Proc. Conf. Corrosion-Erosion Behavior of Materials* (Eds: K. Natesan), St. Louis, Missouri **1978**, p. 162.

[8] J. B. Zu, G. T. Burstein, I. M. Hutchings, *Wear* **1991**, *149*, 73.

[9] A. K. Cousens, I. M. Hutchings, *Wear* **1983**, *88*, 335.

[10] J. Salik, D. Buckley, W. A. Brainard, *Wear* **1981**, *65*, 351.

[11] W. A. Brainard, J. Salik, *NASA Technical Paper 1609*, Lewis Research Center, Cleveland, OH **1980**.

[12] J. W. Edington, I. G. Wright, *Wear* **1978**, *48*, 131.

[13] G. P. Tilly, W. Sage, *Wear* **1970**, *16*, 447.

[14] J. H. Neilson, A. Gilchrist, *Wear* **1968**, *11*, 111.

[15] Deutsches Institut für Normung e.V., *DIN EN 573-3:2019-10, Aluminium and Aluminium alloys–Chemical Composition and Form of Wrought Products*, Beuth-Verlag, Berlin **2019**.

[16] M. Seitz, A. Reeb, A. Klumpp, K. A. Weidenmann, *KEM* **2017**, *742*, 137.

[17] M. Seitz, K. A. Weidenmann in *Lecture Notes in Mechanical Engineering* (Eds.: S. Itoh, S. Shukla), Springer, Singapore, **2020**, p. 10.

[18] L. Spieß, G. Teichert, R. Schwarzer, H. Behnken, C. Genzel, *Moderne Röntgenbeugung. Röntgendiffraktometrie für Materialwissenschaftler, Physiker und Chemiker*, Vieweg & Teubner, Wiesbaden, Germany **2019**, Ch. 8.

[19] G. K. Williamson, W. H. Hall, *Acta Metall.* **1953**, *1*, 22.

[20] T. P. D. Rajan, R. M. Pillai, B. C. Pai, *J. Mater. Sci.* **1998**, *33*, 3491.

[21] G. K. Williamson, R. E. Smallman, *Philos. Mag.* **1956**, *1*, 34.

[22] K. P. D. Lagerlöf, A. H. Heuer, J. Castaing, J. P. Riviére, T. E. Mitchell, *J. Am. Ceram. Soc.* **1994**, *77*, 385.

[23] B. J. Hockey, *J. Am. Ceram. Soc.* **1971**, *54*, 223.

[24] I. A. Cutter, R. McPherson, *J. Am. Ceram. Soc.* **1973**, *56*, 266.

[25] D. Lewis, E. J. Wheeler, *J. Mater. Sci.* **1969**, *4*, 681.

[26] E. K. Beauchamp, M. J. Carr, R. A. Graham, *J. Am. Ceram. Soc.* **1985**, *68*, 696.